I&EC research
Industrial & Engineering Chemistry Research

pubs.acs.org/IECR
Article

NH_3-SCR-DeNO$_x$ Activity of Cu-Containing Commercial Zeolite Y

Magdalena Jabłońska,* Rujito S. R. Suharbiansah, Kinga Góra-Marek, Marek Rotko, Monika Ruszak, Muhammad Fernadi Lukman, Ana Palčić, Reinhard Denecke, Marko Bertmer, Jacek Grams, Andreas Pöppl, and Roger Gläser

Cite This: *Ind. Eng. Chem. Res.* 2024, 63, 17075−17085

Read Online

ACCESS | Metrics & More | Article Recommendations | Supporting Information

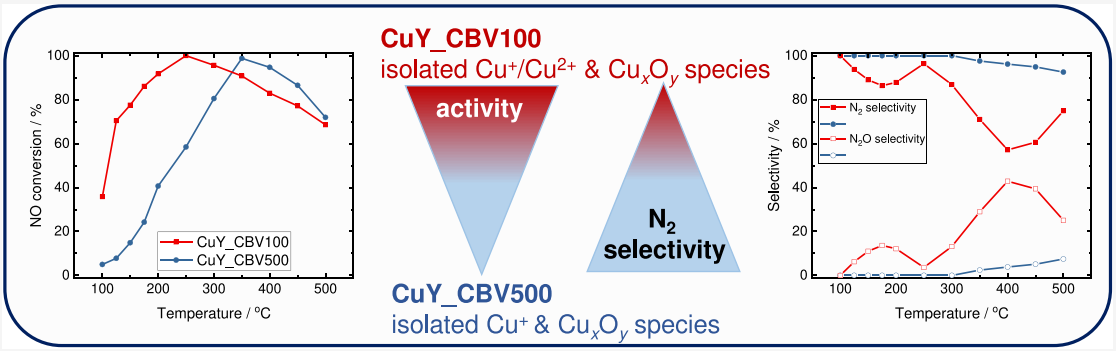

ABSTRACT: Commercial zeolite Y with different n(Si)/n(Al) ratios modified with copper cations were evaluated in the selective catalytic reduction of nitrogen oxide with ammonia (NH_3-SCR-DeNO$_x$). Among the investigated catalysts, the highest activity was achieved over CuY_CBV100 with 7.7 wt % of Cu. The activity of this sample was further confirmed in the feed of the tail gases stream from the pilot HNO_3 plant. The highest N_2 selectivity possesses CuY_CBV500 (3.7 wt % of Cu). To improve catalytic properties, both zeolites were mixed before ion exchange with copper, as well as in a more effective approach, both Cu-containing catalysts were physically mixed (in different weight ratios, 1:1, 1:9, 3:7, 7:3). CuY_CBV100 is more active due to the presence of more active sites, available in reduction/oxidation half-cycles.

1. INTRODUCTION

Nitrogen oxides (NO_x; NO and NO_2) are some of the air pollutants that cause serious human and environmental problems, such as bronchitis, asthma, acid rain, and photochemical smog, etc.[1,2] NH_3-SCR-DeNO$_x$ is the most efficient NO_x removal technology over the Cu-containing catalysts, including Cu-SSZ-13, Cu-SAPO-34, Cu-ZSM-5, etc.[3,4] Among them, Cu-containing zeolite Y or ultrastable zeolite Y (USY) has been less intensively investigated regarding its catalytic properties and the reaction mechanisms in this reaction. However, Ochońska et al.[4] reported more than 80% NO conversion between 150 and 500 °C over Cu-USY (n(Si)/n(Al) = 4.5, 2.4 wt % of Cu). Furthermore, Zhou et al.[5,6] optimized commercially available USY regarding copper content (with the optimum of 5 wt % among 1−12 wt %) and the addition of Ce promoter (8 wt %). Also, the USY-based catalysts revealed enhanced activity and stability in the selective catalytic oxidation of ammonia (NH_3-SCO).[7] Our recent results[8,9] revealed enhanced activity over Cu-containing zeolite Y-based catalysts. Furthermore, as prepared (n(Si)/n(Al) = 1.6, 8.2 wt % of Cu) and commercially based (n(Si)/n(Al) = 2.29, 6.5 wt % of Cu) zeolite Y catalysts revealed comparable NO conversion. Therefore, intensive studies over commercially available zeolite Y are worth investigating to optimize its activity in NH_3-SCR-DeNO$_x$ at extended operation temperature windows. Moreover, the investigation of the reaction mechanisms over Cu-containing zeolite Y samples needs further exploration.

Thus, in the present studies, a series of commercially available zeolite Y samples were modified with copper cations, fully characterized in terms of their physicochemical properties, and further evaluated for the NH_3-SCR-DeNO$_x$ activity and N_2 selectivity.

Besides conventional zeolite Y (CBV100), mildly or severely steamed as well as acid treated materials were applied (CBV500, CBV720, CBV760, CBV780, and CBV901). Steaming facilitates the dealumination of the framework while maintaining the bulk n(Si)/n(Al) ratio unchanged, while treatment with acid is applied to remove extra-framework

Received: June 15, 2024
Revised: September 13, 2024
Accepted: September 17, 2024
Published: September 27, 2024

Al from the steamed zeolites. Furthermore, by steaming and subsequent acid leaching, mesopores are formed, which enhances the adsorption of copper species on the surface of porous zeolite Y (e.g.,[10,11]). The activity and stability of the selected sample were evaluated in the feed of the tail gas stream from the pilot HNO_3 plant. The reaction mechanism was evaluated via temperature-programmed methods, steady-state isotopic transient kinetic analysis (SSITKA), and *in situ* FT-IR. Thus, this work intensifies the development of competitive zeolite Y-based catalysts with high application potential.

2. EXPERIMENTAL SECTION

2.1. Catalyst Preparation. Commercially available zeolite Y samples were purchased from Zeolyst (Table 1). Before modification, the as-received zeolite Y samples (CBV*X*) were calcined (at 550 °C for 4 h in static air with a heating rate of 1 °C min^{-1}). Our approach was dictated by economic considerations, i.e., the use of zeolites available commercially without any other modification. After that, they were ion-exchanged using a 0.05 M aqueous solution of copper(II) acetate (≥98 wt %, Alfa Aesar) at room temperature (ca. 25 °C) for 24 h (1 g of zeolite per 100 mL of copper precursor solution). After 24 h of stirring, the copper-containing zeolite Y samples were filtered and thoroughly washed until pH 7 was reached, then dried and calcined at 550 °C for 4 h in static air (with a heating rate of 1 °C min^{-1}), resulting in the samples named CuY_CBV*X*. In the further approach, calcined Cu-containing CuY_CBV100 and CuY_CBV500 samples were mixed in the weight ratio of 1:1, 1:9, 3:7, and 7:3. As prepared materials were mixed in a mortar, pressed, and crusted to the size of 200−400 μm. For comparative purposes, calcined pure zeolites CBV100 and CBV500 were mixed in the same weight ratios (1:1, 1:9, 3:7, and 7:3) and then subjected to an ion-exchange procedure using a 0.05 M aqueous solution of copper(II) acetate. After modifications with copper species, the samples were washed, dried, calcined, and finally crusted to a size of 200−400 μm. Samples are called CuY-(CBV100+CBV500).

Table 1. Data Declared by the Producers of Commercially Available Zeolites Applied in These Studies[a]

Sample	Form	n(Si)/n(Al)	Treatment[13]
CBV100	Na^+	2.55	parent zeolite
CBV500	NH_4^+	2.6	ion-exchanged, mildly steamed
CBV720	H^+	15	ion-exchanged, severely steamed, acid treated
CBV760	H^+	30	ion-exchanged, severely steamed, acid treated
CBV780	H^+	40	ion-exchanged, severely steamed, acid treated
CBV901	H^+	40	ion-exchanged, severely steamed, acid treated, heat treated

[a] n(Si)/n(Al) values are provided by the producer.

2.2. Granulates Preparation. For the catalytic studies in the feed of tail gas stream from the pilot HNO_3 plant in Puławy (Poland), the CuY-CBV100 catalyst powder was processed into granules. Therefore, 60 g of the catalyst powder was mixed in a mortar with 15 g of AlO(OH) sol (solid fraction 24.0 wt %), 1.8 g of ethylene glycol (Merck, Germany), 0.9 g of Optapix (poly(vinyl alcohol) compound, Zschimmer & Schwartz, Germany), and water until a homogeneous, paste-like mass was obtained. The sticky paste was molded into thin stripes on a glass plate using a syringe. After drying, the stripes were cut down into small granules and sieved to a particle size fraction between 1.0 and 1.5 mm. Finally, the granules were calcined for 1 h at 400 °C at a heating rate of 2 °C min^{-1}. The used AlO(OH) sol was prepared in advance by mixing 270 g of boehmite powder (Dispersal, Sasol Germany) with 576 mL of water and 54 mL of 2 M HNO_3. The suspension was dispersed at 8000 rpm for 10 min by an Ultra turrax. A highly viscous gel was obtained after a few days of resting at room temperature under ambient conditions with a solid fraction of 24.0 wt %.

2.3. Catalyst Characterization and Catalytic Experiments. The zeolite Y and Cu-containing zeolite Y samples (CuY) were characterized concerning the structure and morphology (XRD, NMR and SEM), elemental analysis (ICP-OES, XPS), surface composition (ToF-SIMS), texture (N_2 sorption), and the nature of copper species (DR UV−vis, TPR-H_2, EPR), and examined for their catalytic activity and N_2 selectivity in the NH_3-SCR-DeNO_x. The most active catalyst was evaluated in the form of granulates in the real tail gases from the pilot nitric acid plant. Additional tests of selective ammonia oxidation (NH_3-SCO) and N_2O decomposition (deN_2O) were also implemented. Furthermore, the reaction mechanism was thoroughly evaluated *via in situ* spectroscopy (rapid scan FT-IR), temperature-programmed, and transient techniques (steady-state transient isotopic analysis, SSITKA).

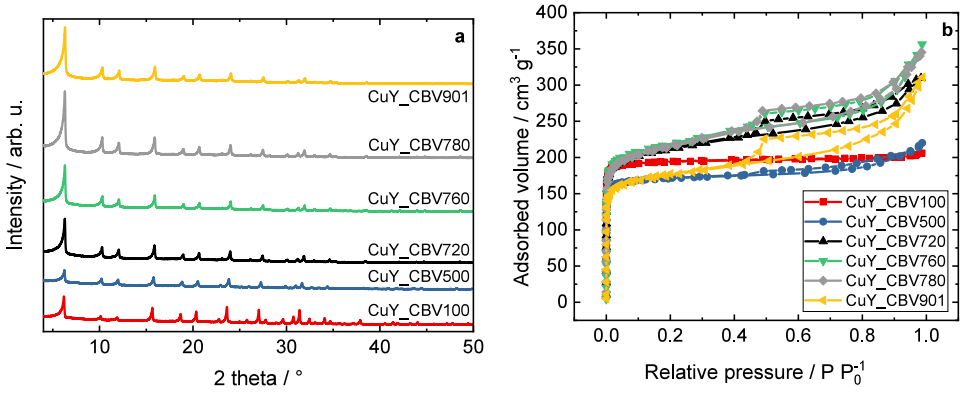

Figure 1. a) XRD patterns and b) N_2 sorption isotherms of Cu-containing zeolite Y samples.

https://doi.org/10.1021/acs.iecr.4c02245
Ind. Eng. Chem. Res. 2024, 63, 17075−17085

Table 2. Elemental Composition and n(Si)/n(Al) and n(Cu)/n(Al) Ratios of Cu-Containing Zeolite Y Samples[a]

Sample	ω_{Al}/wt.-%	ω_{Si}/wt.-%	ω_{Na}/wt.-%	ω_{Cu}/wt.-%	n(Si)/n(Al)	n(Cu)/n(Al)
CuY_CBV100	8.2	21.2	2.2	7.7	2.5/2*	0.4
CuY_CBV500	9.1	24.5		3.7	2.6/2*	0.2
CuY_CBV720	2.7	37.0		2.4	13.2/20*	0.4
CuY_CBV760	1.4	37.2		2.8	25.5/35*	0.8
CuY_CBV780	0.9	38.0		3.4	40.6/40*	1.6
CuY_CBV901	1.6	38.9		2.3	23.4/25*	0.6

[a] ω_i: mass fractions; * obtained from XPS analysis.

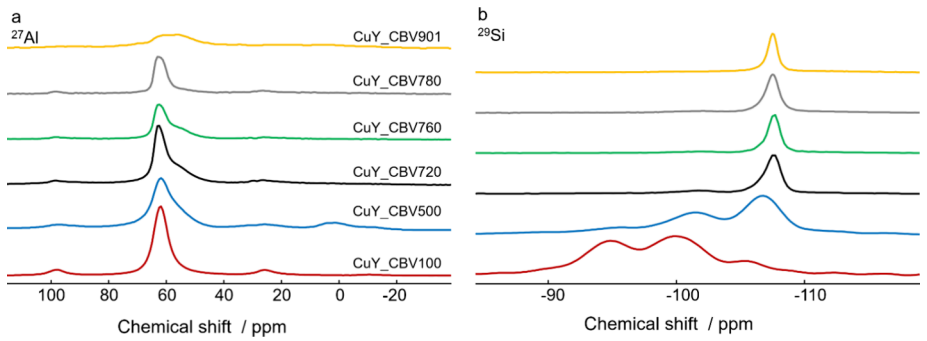

Figure 2. a) ^{27}Al MAS, b) ^{29}Si MAS spectra of Cu-containing Y samples.

The details of the experimental procedure can be found in the Supporting Information.

3. RESULTS AND DISCUSSION

3.1. Structural, Morphological, and Textural Properties. The powder XRD patterns of the Cu-containing zeolite Y materials (Figure 1a) match well with the patterns of the respective calcined zeolite Y samples (Figure S1a) in terms of the position of characteristic peaks corresponding to FAU-type framework materials at 2θ of 6.3°, 10.3°, 12.2°, 16°, 19.1°, 20.7°, 23.3°, 24.1°, 27.6°, etc., as well as preserved intensity of the diffraction patterns. This indicates the high crystallinity degree of the prepared Cu-containing materials (Figure 1a, Figure S1a). Similarly, the values of micropore volume of the Cu-modified zeolite Y samples match well the ones corresponding to the respective parent samples, once again suggesting that the crystal structure and pore structure of the materials are preserved upon Cu-exchange (Table S1, Figure 1b, Figure S1b-d). On the other hand, a difference exists in the mesopore volume and specific surface area between the starting and treated materials, likely due to the partial dissolution of certain less ordered fragments within the zeolite particles in the weakly acidic solution of copper(II) acetate. This phenomenon can be attributed to zeolite framework demetalation, specifically dealumination, as reported in the early days of zeolite science; another important outcome of this process is the formation of intracrystalline mesopores.[14] Furthermore, studies have shown that even with low degrees of dealumination in mildly acidic media, zeolite Y exhibits significant changes in mesoporosity.[10] The results from the chemical analysis of the Cu−Y samples conducted in this study support these conclusions, as the measured n(Si)/n(Al) values closely resemble those of the initial materials (Table SI2 and Table 2). This once again supports the conclusion that modification with the Cu species does not significantly affect the zeolite Y material. However, please note that the values for CBV910 and CuY_CBV901 deviate significantly from the data declared of the manufacturer.[12] The observed n(Si)/n(Al) values obtained by XPS mainly confirm the ICP results. However, due to the overlap of core levels and rather large differences in the individual quantities the values have large error bars (about ±20% of the values). The amount of Cu for most samples (except the CuY_CBV100) is at the edge to be seriously quantified. SEM images of the Cu-containing samples (Figure S2) show that the zeolite Y particles are composed of intergrown crystals with sharp edges. The tendency toward agglomeration seems to be more expressed in the samples CuY_CBV100, CuY_CBV500, and CuY_CBV720, while in the samples CuY_CBV760, CuY_CBV780, and CuY_CBV901 more isolated crystals are observed. In addition, the latter samples present larger intergrowths with less pronounced edges of the forming crystals. The size of the majority of the particles lies in the range of 600−1100 nm, whereas the maximum of the curve varies without a clear trend, can be explained by the uncertainty of the particles size determination on the grounds of the image analysis. Namely, the number of particles analyzed in this way is around 100.

Furthermore, ^{27}Al MAS NMR spectra (Figure 2a) display that most Al atoms in all the Cu-containing samples reside in framework T positions, as revealed by the signal at ca. 62 ppm. However, additional resonances for other four-coordinated signals (CuY_CBV500, CuY_CBV720, CuY_CBV760, and CuY_CBV901), five-coordinated signals (CuY_CBV100, CuY_CBV500, and CuY_CBV720) as well as six-coordinated signals in CuY_CBV500) demonstrate that a certain amount of Al is extracted from the zeolite framework tetrahedral positions by postsynthetic modifications of native zeolite Y, yet retained within the material upon treatment with copper(II) acetate. ^{29}Si MAS NMR spectra shown in Figure 2b, reflect the framework positions of Si in the FAU-type material. Samples CuY_CBV100 and CuY_CBV500 show the expected signals at −94, −99, and −104 ppm for Q^4(2Al), Q^4(1Al), and Q^4(0Al), respectively.[15,16] Although both samples have similar n(Si)/n(Al) ratios, the relative intensities of the three peaks differ significantly. This is due to the fact that in the sample CuY_CBV500 a significant portion of Al moieties are not fully

https://doi.org/10.1021/acs.iecr.4c02245
Ind. Eng. Chem. Res. 2024, 63, 17075−17085

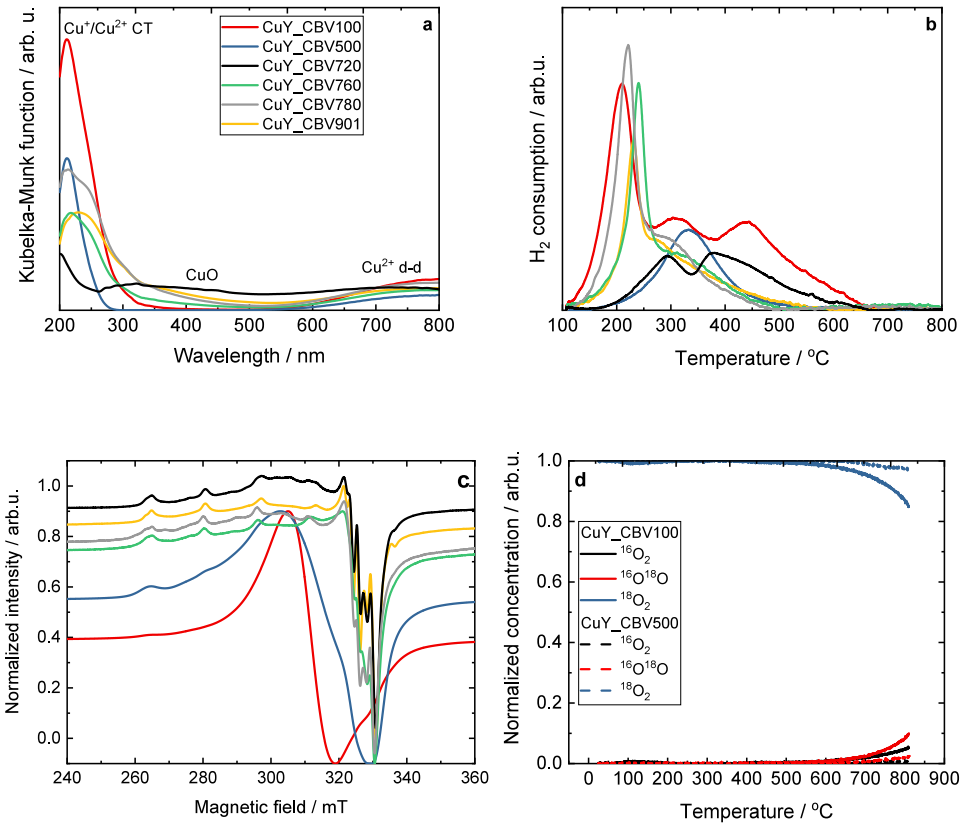

Figure 3. a) DR UV−vis spectra, b) TPR-H_2 profile for Cu-containing zeolite Y samples, and c) CW-EPR spectra of the activated samples recorded at −196 °C; (a,c) the sample names are the same; d) TPIE profile for selected Cu-containing zeolite Y samples.

attached to the framework, as confirmed by the ^{27}Al MAS NMR spectrum, which shows several additional signals (^{27}Al MQMAS spectrum, Figure S3) corresponding to tetrahedral sites with well-defined environment as well as five- and six-fold coordinated Al species. All of the other samples show a single ^{29}Si peak at −107 ppm. Since these samples have a high n(Si)/n(Al) ratio a slight shift of the Q^4(0Al) feature to more negative values occurs.[17] One possible explanation for the observed behavior could be attributed to the CBV100 sample serving as the parent sample for all other CBV samples examined in this study. However, they vary in the extent of the steaming treatment they underwent.[13]

3.2. Nature of Copper Species. The nature of copper species varied significantly, depending on the applied zeolite Y. Figure 3a shows the DR UV−vis spectra of the analyzed samples. CuY_CBV100 possessing the highest amount of copper revealed also the highest amount of isolated Cu species. Relatively narrow peaks, indicating isolated Cu species, appear also for the CuY_CBV500 sample. Other samples possessed mainly more aggregated copper species. Nevertheless, EPR studies excluded the presence of $[Cu-O-Cu]^{2+}$ species. Also, in our previous studies about Cu-containing zeolite Y we did not observe NO to NO_2 oxidation over $[Cu-O-Cu]^{2+}$ species during TPD-NO.[8] The heterogeneity of these species is also reflected by the TPR-H_2 profiles (Figure 3b). The copper species in CuY_CBV100 are reduced in three clear stages, while in CuY_CBV500 only one reduction peak appears, whereas, for other samples, mainly two stages of reduction appeared. According to Kieger et al.,[18] the copper species located in supercage are reduced below 300 °C, while the species located in sodalite cages are reduced above 300 °C. On the other hand, Wang et al.[19] reported that the Cu^{2+} species are reduced below 300 °C, while Cu^+ species are reduced above 300 °C. However, according to the data gathered in Figure 3b, the reduction of the copper species varied significantly among applied zeolites, and thus, the reduction stages cannot be clearly assigned. Such differences in DR UV−vis and TPR-H_2 profiles among other samples are connected with their modification procedures (Table 1), and thus, resulting in variation in n(Si)/n(Al) ratios (i.e., increasing amount of Si) as well as textural properties (i.e., introduced mesopores). Overall, both steamed and acid treated samples possess a higher amount of aggregated copper species. Though, based on DR UV−vis and TPR-H_2 profiles, we found that CuY_CBV100 possesses mainly isolated Cu^+/Cu^{2+} and Cu_xO_y species, while the Cu^+ and Cu_xO_y species are the main centers in CuY_CBV500, which is also supported by our previous studies (including room temperature CO and NO adsorption experiments).[8,20] Furthermore, EPR studies (see below) confirmed the coordination of Cu^{2+} with the oxygen zeolite lattice. Due to the low Cu content, XPS data cannot contribute to the assignment of Cu species, except for CuY_CBV100 for which contributions of both Cu^+ and Cu^{2+} are observed.

Figure 3c and Figures S4 and S5 display a series of CW-EPR spectra of calcined (Figure S4) and activated (Figure 3c and Figure S5) samples, while Table S3 provides the comparison of relative EPR intensities for all calcined samples. Upon the activation procedure at 200 °C for 2 h under a high vacuum (i.e., 10^{-6} mbar), Cu^{2+} speciation evolves differently for all Cu-containing zeolite Y samples. The summary of Cu^{2+} spin Hamiltonian parameter according to the spectral simulation (Figure S4) analysis is given in Table S4 and the composition

https://doi.org/10.1021/acs.iecr.4c02245
Ind. Eng. Chem. Res. 2024, 63, 17075−17085

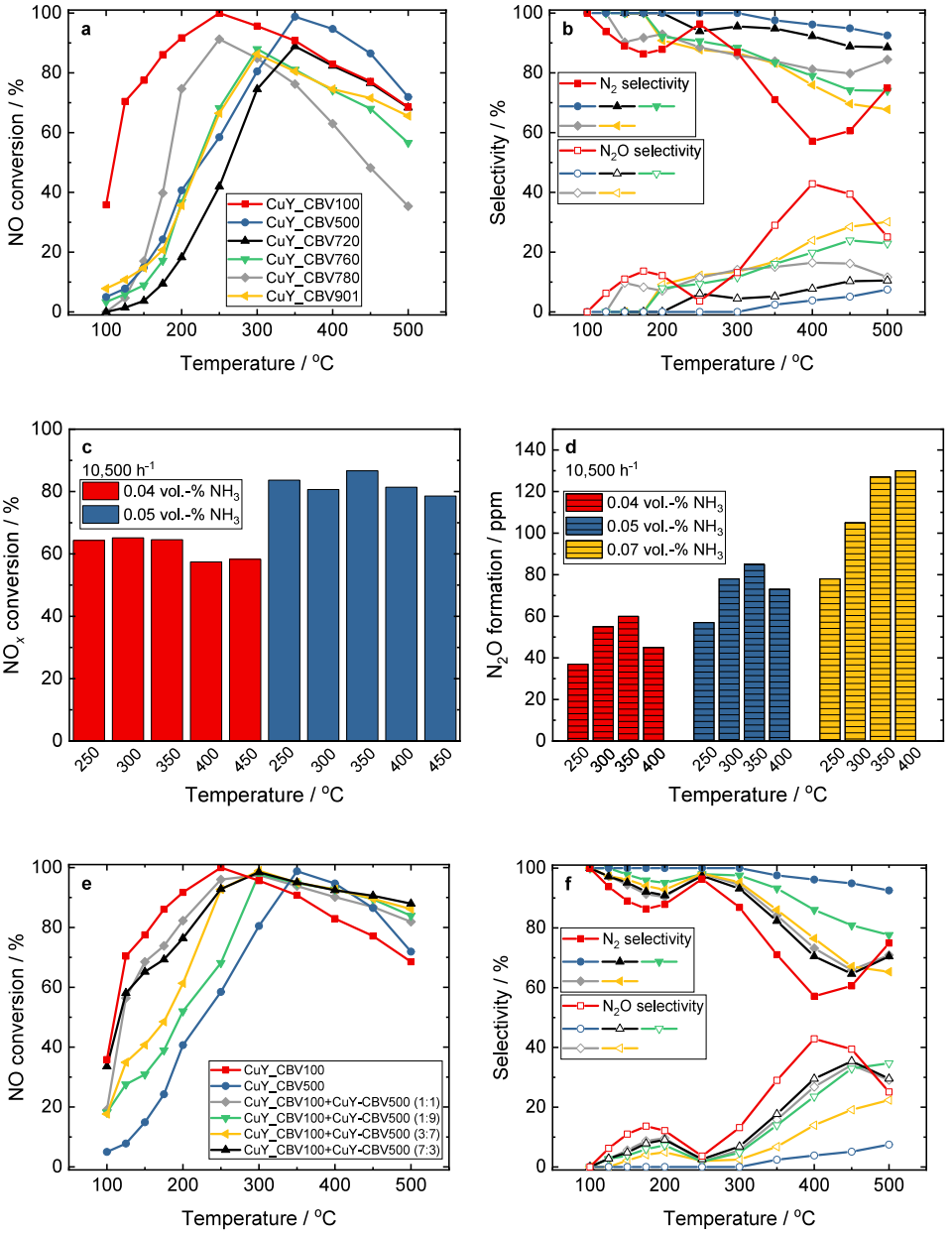

Figure 4. a,e) NO conversion and b,f) N_2, N_2O selectivity during NH_3-SCR-DeNO$_x$ over Cu-containing Y samples. Reaction conditions: m_K = 0.1 g, c(NO) = 0.1 vol.-%, $c(NH_3)$ = 0.1 vol.-%, $c(O_2)$ = 5 vol.-%, He balance, F_{TOT} = 120 mL min^{-1}, GHSV = 30,000 h^{-1}, a,b) and c,d) the sample names are the same. c) NO$_x$ conversion and d) N_2O formation during NH_3-SCR-DeNO$_x$ over CuY_CBV100 in the feed of tail gases stream from the pilot HNO_3 plant. Reaction conditions: m_G = 26 g, c(NO$_x$) = 0.072 vol.-%, $c(NH_3)$ = 0.04−0.07 vol.-%, $c(O_2)$ = 3.8 vol.-%, GHSV = 10,500 h^{-1}.

of each species are collected in Table S5. Specifically, for the most active sample (CuY_CBV100 (n(Si)n(/Al) ratio of 2.5, Cu content of 7.7 wt.-%) in the NH_3-SCR-DeNO$_x$, the line width is still very broad (g_{iso} = 2.17) with a tiny portion of unresolved hyperfine lines (Figure 3c). The isotropic species E arises from the dipole−dipole exchange interactions between Cu^{2+} ions in high local concentrations.[8] The most N_2 selective in NH_3-SCR-DeNO$_x$ (CuY_CBV500 sample with a n(Si)/n(Al) ratio of 2.6 and total Cu content of 3.7 wt.-% exhibits more anisotropic species (contribution of around 70%) which can be identified as fully dehydrated Cu^{2+} species (here is labeled as species D, g_{zz} = 2.33 and A_{zz} = 520 MHz). However, well-resolved hyperfine lines at both g_{zz} and $g_{xx,yy}$ region are observed for lesser Cu content and higher n(Si)/n(Al) ratio samples (n(Si)/n(Al) ratio of 23.4, 25.5, and 13.2 for CuY_CBV901, CuY_CBV760, and CuY_CBV720, respectively). In this case, species C (≤15% contribution) should also be considered in the spectral simulation of the CuY_CBV901, CuY_CBV760, and CuY_CBV720 samples. Bruzzese et al.[21] attributed this spin Hamiltonian parameter of species C to four-fold $[Cu(OH)(O_f)_3]^+$ species on the eight-membered ring. Please note that this species also appeared in their case only if the n(Si)/n(Al) ratio is >12 in Cu-containing chabazite zeolites. Last, CuY_CBV780 with the highest n(Si)/n(Al) ratio of 40.6 exhibits around 25% of species C (also the highest species C contribution if compared to the rest of the samples), as indicated from the spectral simulation. Specifically, the Q-band CW-EPR result in Figure.SI4e for the activated

https://doi.org/10.1021/acs.iecr.4c02245
Ind. Eng. Chem. Res. 2024, 63, 17075−17085

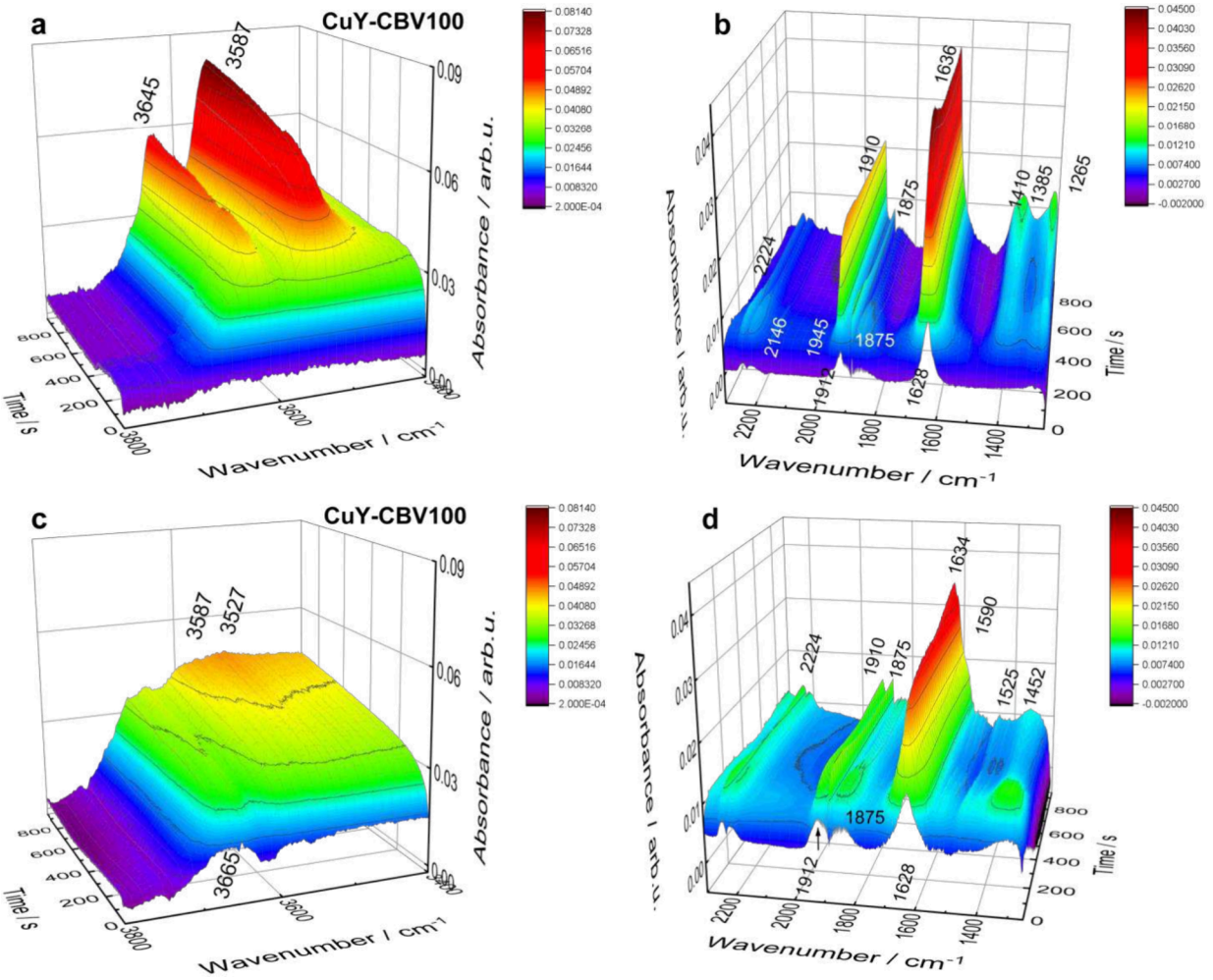

Figure 5. Time-resolved rapid scan FT-IR differential spectra presenting the gaseous and surface-bonded species involved in NH_3-SCR-DeNO$_x$ at 125 °C over CuY_CBV100 (a,b) and CuY_CBV500 (c,d) in the presence of water vapor in 950 s reaction course in the stretching N−H modes (a,c) and the frequency region typical for deformation modes of the NO_x^- and NH_3-originated species (b,d).

CuY_CBV100 sample ruled out the presence of $[Cu{-}O{-}Cu]^{2+}$ species since the spectral pattern only shows a broad peak centered at 1118 mT (g_{iso} = 2.16) due to species E and the minor Cu^{2+} monomer (species D) in line with the result of CW-EPR at X-band frequency. Figure 3d presents the results of temperature-programmed isotopic exchange (TPIE) studies carried out over selected samples. The TPIE results revealed that oxygen from the lattice of CuY_CBV100 is exchanged with oxygen ($^{18}O_2$) from the gas phase. A significantly lower effect is observed over CuY_CBV500, which can be attributed to the restricted mobility of lattice oxygen in this sample.

3.3. Catalytic Studies. Cu^{2+} species serve as active centers for low temperature during NH_3-SCR-DeNO$_x$, while CuO species cause NH_3 oxidation above 350 °C. The presence of Cu^+ and CuO species lead to lower NO conversion during reaction; however, their lower reducibility enhances material' selectivity to N_2. Thus, Cu^{2+} and Cu^+ species present in the sample boost low-temperature activity together with N_2 selectivity in the high-temperature range. This can be achieved in one materials by appropriate synthesis steering, as we have shown in our previous studies,[22] or by the preparation of mixed materials.

Figure 4 presents the catalytic activity results over Cu-containing zeolite Y samples in the NH_3-SCR-DeNO$_x$. Among the investigated Cu-containing Y catalysts, the sample with a n(Si)/n(Al) ratio of 2.55 reached more than 80% NO conversion in the temperature range of 175−400 °C. The NO conversion significantly drops above 300 °C due to NH_3 oxidation (Figure S6a,b). This effect is less pronounced for CuY_CBV500, which also showed the highest N_2 selectivity among the investigated materials (Figure 4b). Thus, NO conversion was favored over materials containing isolated Cu^{2+} species, while N_2 and N_2O selectivity was favored over catalysts containing Cu^+ and Cu_xO_y species, respectively. The formation of N_2O below 250 °C primarily results from the decomposition of NH_4NO_3.[9] Above 350 °C, N_2O is produced due to the nonselective oxidation of NH_3 (Figure S6b). Compared to Cu-SSZ-13, Cu-ERI, and Cu-ZSM-5 reported in our last studies,[23] Cu-containing zeolite Y possess lower NO conversion and N_2 selectivity between 100 and 500 °C.

The activity of the CuY_CBV100 catalysts was further evaluated in the feed of the tail gas stream from the pilot HNO_3 plant in Puławy (Poland). The industrial application requires the shaping of this catalytic material. After the sample was aged in the feed (including NH_3) for 1 week, the measurements were carried out. As can be seen from Figure 4c,d, and Figure S7, in addition to the NO_x conversion, N_2O formation was monitored. The comparison of the NO_x

https://doi.org/10.1021/acs.iecr.4c02245
Ind. Eng. Chem. Res. 2024, 63, 17075−17085

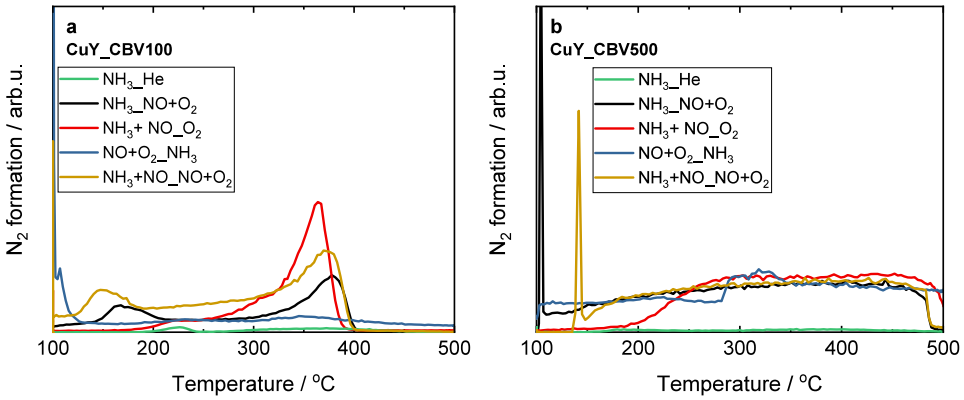

Figure 6. Formation of N_2 during temperature-programmed studies over a) CuY_CBV100 and b) CuY_CBV500. Reaction conditions: pretreatment in He, m_K = 0.1 g; adsorption: given species at 100 °C, purged in He, F_{TOT} = 50 mL min^{-1}, 'desorption: in flow of the given species, F_{TOT} = 50 mL min^{-1}, linear heating rate of 10 °C min^{-1}; c(NO) = 0.3 vol.-%, c(NH_3) = 0.3 vol.-%, c(O_2) = 10 vol.-%, He balance. Labels refer to "adsorption_desorption".

conversion for the different flow rates revealed higher conversion at a gas flow rate of 10,500 h^{-1} than at 13,300 h^{-1}. In the latter case, the contact time of reactants with the catalyst surface was shorter for effective reduction of the amount of NO_x with ammonia. The change in N_2O concentration in the tail gas stream indicates that the oxidation of ammonia occurred in the presence of the catalyst, i.e., the amount of N_2O formed was proportional to the amount of ammonia added to the feed (Figure 5d, Figure S7b). The structure and textural properties of zeolite Y were not affected after catalytic tests under pilot plant operating conditions during the two week test (Figure S8), indicating its high stability.

Table S6 shows the intensity ratios of selected ions calculated on the basis of the collected ToF-SIMS spectra. The obtained results indicate an increase in the intensity of copper in relation to those of silicon and aluminum for the sample after the reaction. Moreover, in the same case, a slight decrease in the intensity of aluminum relative to silicon can also be observed, which can indicate partial segregation of Cu species on the zeolite surface. Still, there are no significant differences between the fresh granulates and after the reaction (Figure S8c). Furthermore, the catalytic studies over fresh and used granulates (Figure S9) revealed no significant differences in conversion or selectivity in NH_3-SCR-DeNO$_x$ and NH_3-SCO.

Furthermore, to seek a balance between NH_3-SCR-DeNO$_x$ activity and N_2 selectivity, in the next step, we mixed CuY_CBV100 and CuY_CBV500 in weight ratios of 1:1, 1:9, 3:7, and 7:3, respectively. Also, for comparative purposes, we mixed pure calcined CBV100 and CBV500 with the same weight ratios of 1:1, 1:9, 3:7, and 7:3. Such mixed zeolite samples were further modified with copper species. The activity and N_2 selectivity depend on the applied methods of introducing Cu species (Figure 4e,f, for mixed CuY_CBV100+CuY_CBV500 samples and Figure S10 for Cu-exchanged CuY(CBV100+CBV500) samples). However, as a more efficient approach, the physical mixture of Cu-containing samples is recognized, which is represented by the higher activity and N_2 selectivity of the samples compared to the analogous samples obtained by the physical mixture of pure calcined zeolites and subsequently ion exchanged with Cu species. Overall, the mixtures with a higher content of CuY_CBV100 than CuY_CBV500 revealed higher activity and N_2 selectivity above 300 °C in comparison to pure CuY_CBV100. The same conclusion is given for the catalysts based on mixed pure zeolites, which are subsequently Cu-exchanged (Figure S10).

Figure 5 displays the FT-IR spectra of the zeolites CuY_CBV100 and CuY_CBV500 during NH_3-SCR-DeNO$_x$ at 125 °C (c(NH_3):c(NO):c(O_2):c(H_2O) = 4:4:1:8). The spectra were collected over a 950 s reaction course in rapid scan mode by collecting one spectrum in 0.8 s. The spectral region of the O−H stretching vibrations (Figure 5a,c) arises due to the νO−H symmetric mode and its splitting by adsorption on active sites. The interaction of NO with copper sites and its subsequent conversion are detected in the lower wavenumber range (2300−1250 cm^{-1}) (Figure 5b,d). Solely, the copper(II) mononitrosyl bands appear at 1945 and 1912 cm^{-1} in CuY_CBV100 (Figure 5b). Both nitrosyl species are overlapped by the oscillation-rotational spectrum of gaseous NO, which is also easily identified by the 1875 cm^{-1} band. The Cu^{2+}(NO) bands at 1945 and 1912 cm^{-1} are assigned to isolated Cu^{2+} cations possessing an adjacent OH^- anion (i.e., the structure of the adsorption site is [Cu(OH)]$^+$).[9,24,25] The Cu(II) mononitrosyl band at 1945 cm^{-1} is rapidly eroded within the first 120 s of reaction duration while the lower frequency mononitrosyl band at 1912 cm^{-1} develops in time until 400 s. Then its decline is observed, accompanied by gaseous NO consumption. Solvation by ammonia confers mobility to Cu(II) significantly, thus enhancing the accessibility of Cu^{2+} cations for the reagent molecules. The Cu^{2+} cations, if withdrawn by ammonia from sodalite cages to the supercages, react with NO molecules forming [Cu(OH)-$(NH_3)_n$]$^+$ complexes. In the case of CuY_CBV100, an obvious time dependence is observed: Only [Cu(OH)$(NH_3)_n$]$^+$ adducts located in supercages can ligate NO molecules immediately (1945 cm^{-1}), and they are consumed in NH_3-SCR-DeNO$_x$ as the first. The [Cu(OH)$(NH_3)_n$]$^+$ species formed on the Cu^{2+} cations originally located in sodalite cages and being withdrawn by ligation to ammonia are represented by the increase of the band intensity at 1910 cm^{-1} over the first 450 s, and then they are also consumed over a time. The ligation of NO to [Cu(OH)$(NH_3)_n$]$^+$ is also reflected in the development of the nitrate/nitrite bands in the 1636−1250 cm^{-1} wavenumber region. The bending modes of NH_3-Lewis adducts also contribute to these by the complex bands. In parallel with the bands at 1945 and 1912 cm^{-1}, the δ_{asym} NH_3

https://doi.org/10.1021/acs.iecr.4c02245
Ind. Eng. Chem. Res. 2024, 63, 17075−17085

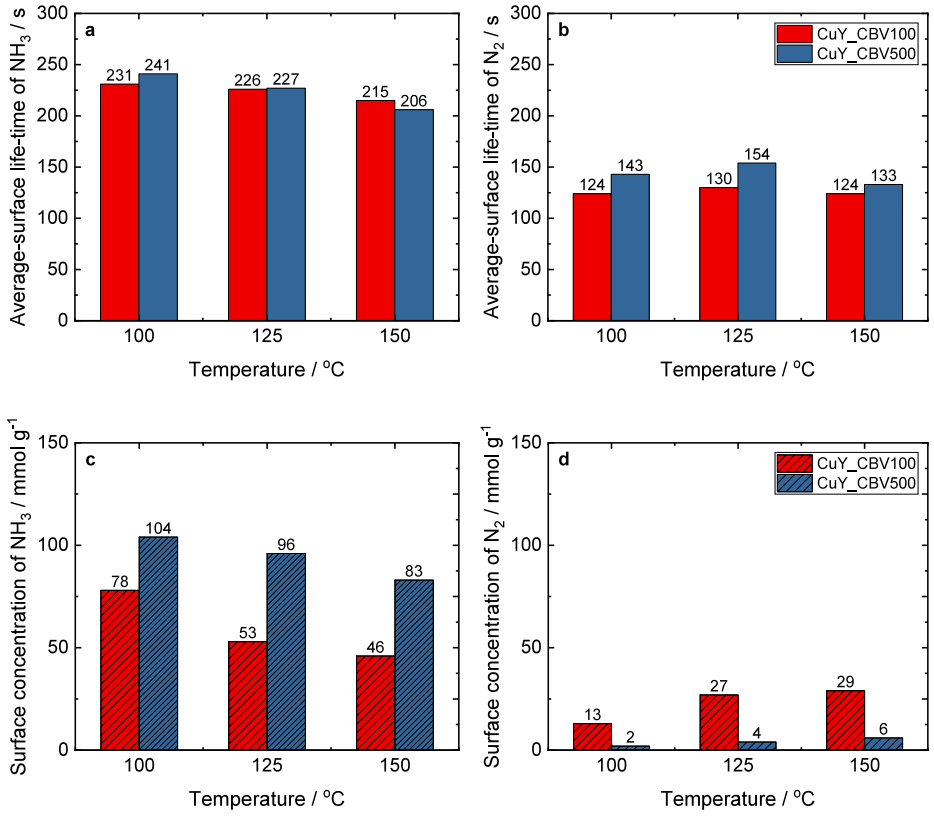

Figure 7. a,b) Average-surface lifetime of reversibly adsorbed ammonia, adsorbed nitrogen molecules, and intermediates leading to the formation of nitrogen, and (c,d) surface concentration of reversibly adsorbed ammonia, adsorbed nitrogen molecules, and intermediates leading to the formation of nitrogen.

band appears at 1628 cm^{-1}, so it can be assigned to the ammine ligands in $[Cu(OH)(NH_3)_n]^+$ complexes. This band increases for the first 450 s of the process, and then its gradual decrease is observed, associated with consuming mononitrosyls and NO in the gas phase. At the same time, the position of the δ_{asym} band of NH_3 is shifted to the higher wavenumbers (i.e., 1636 cm^{-1}). This allows for anticipation of the mixed complex $[Cu(NH_3)_{n-1}(NO_3)]^+$ formation. The nitrites are identified by the NO_2^- bands at 1410 and 1265 cm^{-1}. These results indicate that during NH_3-SCR-DeNO$_x$, nitrates/nitrites coexist with the copper-ammonia cage complexes in the form of mixed ligand adducts already at the low-temperature stage. Indeed, the $[Cu^{2+}(NH_3)_3(NO_3)]^+$ intermediates were recently reported for Cu-CHA at low reaction temperatures.[26,27] In the course of the reaction, $-NH_2$ (1385 cm^{-1}), NO^+ (2146 cm^{-1}), and N_2O (2224 cm^{-1}) coexist with the $[Cu^{2+}(NH_3)_3(NO_3)]^+$. The domination of nitrates and nitrites in the low-temperature regime (i.e., 125 °C) can be explained by the interaction of NO with isolated Cu^{2+} and Cu^{2+}_{oxo} sites. The dissociative insertion of NH_3 into these species can be anticipated from the presence of the band at 1385 cm^{-1}, characteristic for -NH_2. All these findings indicate that in CuY_CBV100, the isolated Cu^{2+} and mono Cu_xO_y species are responsible for the NH_3-SCR-DeNO$_x$ as they participate in the easy dissociation of NH_3, which is the dominant process at 125 °C.

The IR spectrum of CuY_CBV500 in contact with the SCR reactants at 125 °C (Figure 5c,d) is dominated by the bands around 1634−1622 cm^{-1} discussed above. The situation is, however, different than that in the case of CuY_CBV100 (Figure 6b). The band $[Cu(OH)(NH_3)_n]^+$ at 1912 cm^{-1}, detected as the only mononitrosyl forms, along with the NO_3^- bands around 1525−1452 cm^{-1} which are created in the very early reaction stage, are stable over the SCR process (which was also confirmed via TPD, Figure 6b). Unlike CuY_CBV100, in CuY_CBV500, the intensity of the band at 1634 cm^{-1} characteristic for the mixed ligand adducts $[Cu^{2+}(NH_3)_3(NO_3)]^+$ gradually increases, while the concentrations of the other adsorbed species remain unchanged over time. The contribution of water molecules in this band must be excluded. This can be verified by the intensity of the stretching bands of adsorbed water (Figure 5c), which is only about half that of CuY_CBV100. The declined conversion of nitrate and nitrite complexes $[Cu^{2+}(NH_3)_3(NO_3)]^+$ in final SCR products is responsible for the lower activity of the CuY_CBV500 under these conditions. There are also no bands of -NH_2 (at 1380 cm^{-1}) and NO^+ (at 2146 cm^{-1}, NO^+ is produced on Brønsted acid sites from NO/O_2 mixture with water production),[28] suggesting that the CuY_CBV500 is a less reactive catalyst under these conditions.

The CuY_CBV100 and CuY_CBV500 samples are further investigated regarding the reaction mechanism of NH_3-SCR-DeNO$_x$. Figures S11 and S12 present the results of the temperature-programmed studies (for details, see SI), while Figure 6 shows the formation of N_2 during these studies. Regarding the CuY_CBV100 sample, N_2 is formed below 250 °C as a result of the reaction between adsorbed NH_3 and NO (from the gas phase) (Figure 6a). Also, as N_2 is formed below 150 °C, nitrates act as reactive intermediates in the CuY_CBV100. Finally, N_2 formation between 250 and 400 °C occurs mainly due to unselective NH_3 oxidation over this sample. This is also supported by the higher level of formation of N_2O above 250 °C during NH_3 oxidation (Figure S11b).

https://doi.org/10.1021/acs.iecr.4c02245
Ind. Eng. Chem. Res. 2024, 63, 17075−17085

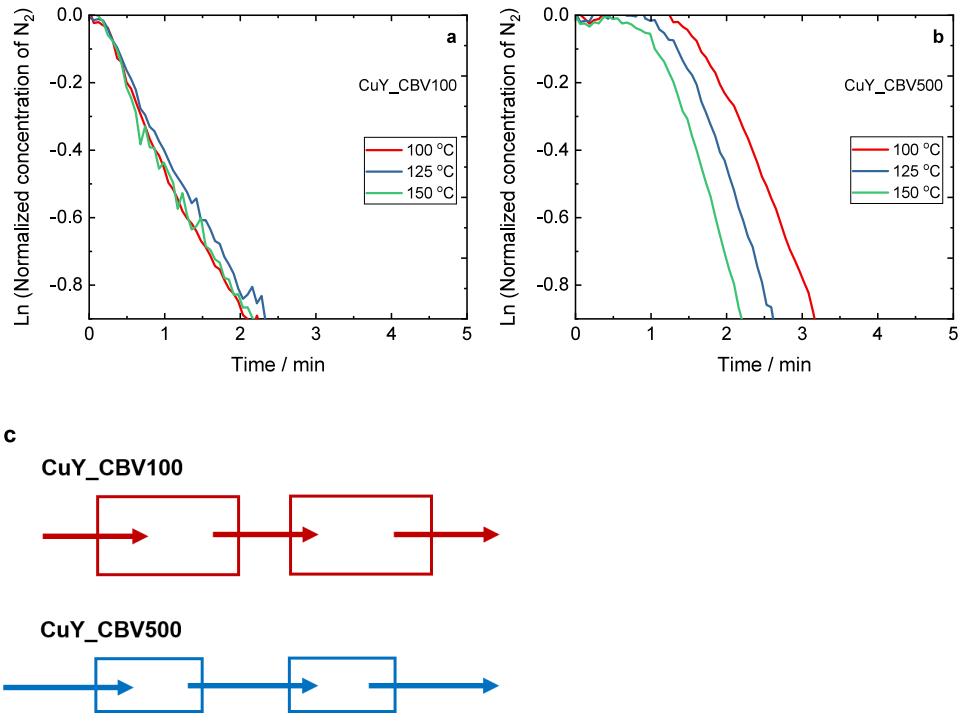

Figure 8. Logarithmic response of $^{14}N_2$ of a) CuY_CBV100 and b) CuY_CBV500, as well as c) a scheme highlighting the mechanism differences between the two catalysts.

Concerning the CuY_CBV500 sample, N_2 is formed in a broad temperature range (Figure 6b), mainly as a result of the reduction of adsorbed nitrates by NH_3 from the gas phase, as well as due to the reduction of adsorbed NH_3 by NO from the gas phase. The sharp peak appearing during the reduction−oxidation cycle (i.e., NH_3+NO_NO+O_2) over this material indicated that the NH_3-SCR-DeNO$_x$ reaction may proceed *via* the HONO intermediates. According to Tronconi et al.,[29] an intense N_2 peak formation during the switch from NH_3 to NO appears as a result of the reduction of *Two-P* (i.e., $[Cu^{II}(OH)(NH_3)_3\cdots Cu^{II}(OH)(NH_3)_3]$ complex) with NO and thus the formation of HONO intermediates. These species further react with NH_3-ligands, forming NH_4NO_2 that decomposes finally into N_2 and H_2O. In the case of the CuY_CBV100 sample, the HONO intermediates appeared below 100 °C and, thus, are not visible.

Figure 7 and Figures S13 and S14 present the results of the SSITKA analysis between 100 and 150 °C for CuY_CBV100 and CuY_CBV500. The delay observed between Ar and $^{14}NH_3$ (or between Kr and $^{15}NH_3$) points out the reversible adsorption of NH_3 on the surface of both catalysts. The average-surface lifetime of NH_3 and its surface concentration (Figure 7a,c) decrease with the increasing temperature. However, the rate of value changes of these two kinetic parameters is different for the studied catalysts. In the case of CuY_CBV100, the value of the average-surface lifetime of reversibly adsorbed ammonia decreases very slowly from 100 to 125 °C, and then faster to 150 °C, while for CuY_CBV500, a stable decreasing trend is observed. Moreover, at 150 °C, the average-surface lifetime of reversibly adsorbed ammonia is shorter on the surface of CuY_CBV500 compared to values obtained at lower temperatures, where it is longer than on CuY_CBV100. However, the differences in the values of the average-surface lifetime of reversibly adsorbed ammonia for both catalysts are not large, whereas the surface concentration of reversibly adsorbed ammonia is significantly higher on the surface of CuY_CBV500 than on CuY_CBV100, especially at 125 and 150 °C. This behavior appears due to the different rates of ammonia consumption in the NH_3-SCR-DeNO$_x$.

Based on the delay between Ar and $^{14}N_2$ (or Kr and $^{14}N^{15}N$), the average-surface lifetime and surface concentration (Figure 7b,d) of nitrogen and intermediates leading to the formation of nitrogen were calculated. The values of average-surface lifetime on the surface of CuY_CBV100 are very similar in the whole range of the studied temperature, while for CuY_CBV500 they varied depending on the reaction temperature being the highest at 125 °C. Moreover, the average-surface lifetime of nitrogen and intermediates leading to the formation of nitrogen is shorter on the surface CuY_CBV100 than on CuY_CBV500, suggesting a higher NH_3-SCR-DeNO$_x$ reaction rate. The surface concentration of nitrogen and intermediates leading to the formation of nitrogen (Figure 7d) calculated for CuY_CBV100 is significantly higher, indicating that there is a higher number of active sites. The differences in the number of active sites between both catalysts are much greater than the differences in their values of average-surface lifetime. This suggests that the higher activity of CuY_CBV100 is mainly due to the larger number of active sites and, to a lesser extent, their higher reactivity. Moreover, the number of active sites is not a constant value but depends on temperature changes.

Figure 8 summarizes the time dependence of the N_2 concentration in a logarithmic plot. In the case of CuY_CBV500, the convexity for the initial N_2 signal after isotopic switching is clearly visible, while for CuY_CBV100 it is less visible. The model of the surface of the CuY catalysts probably consists of pools in series, according to the SSITKA theory.[30,31] This model suggests that more than one intermediate (active sites) is present on the catalyst surface between NH_3 and N_2. The subsequent dehydrogenation of

https://doi.org/10.1021/acs.iecr.4c02245
Ind. Eng. Chem. Res. 2024, 63, 17075−17085

ammonia over catalysts may led to surface nitrogen atoms as follows $NH_3 \rightarrow NH_2 \rightarrow NH \rightarrow N$. Indeed our IR studies revealed presence of -NH_2 form which confirms the dehydrogenation of NH_3 over CuY_CBV100 and CuY_CBV500. Overall, in the case of CuY_CBV100, the pools (well-mixed subsystems within the reaction paths) are larger, while in the case of CuY_CBV500, the time between pools is longer, as shown in Figure 8c.

4. CONCLUSIONS

A series of copper-modified commercial zeolite Y samples were investigated in the NH_3-SCR-DeNO$_x$. Among the investigated samples, the CuY_CBV100 and CuY_CBV500 catalysts revealed high NO conversion and N_2 selectivity, respectively. Both samples possessed the highest amount of isolated copper species, resulting in enhanced catalytic properties. CuY_CBV100 indicated stability in the tail gases stream of the pilot nitric acid plant. The catalytic properties above 300 °C were improved for mixed CuY_CBV100 and CuY_CBV500 catalysts and CuY(CBV100+CBV500) samples. *In situ* FT-IR and TPD studies revealed that nitrites and nitrates also acted as reactive intermediates in NH_3-SCR-DeNO$_x$, while their lower reduction rate proceeded over that of CuY_CBV500.

■ ASSOCIATED CONTENT

Data Availability Statement

The data that has been used is confidential.

Supporting Information

The Supporting Information is available free of charge at https://pubs.acs.org/doi/10.1021/acs.iecr.4c02245.

Experimental and catalytic procedures, additional catalyst characterization and results of catalytic studies, TPD and SSITKA (PDF)

■ AUTHOR INFORMATION

Corresponding Author

Magdalena Jabłońska − *Institute of Chemical Technology, Universität Leipzig, 04103 Leipzig, Germany;* orcid.org/0000-0002-7868-1067; Email: magdalena.jablonska@uni-leipzig.de

Authors

Rujito S. R. Suharbiansah − *Institute of Chemical Technology, Universität Leipzig, 04103 Leipzig, Germany*

Kinga Góra-Marek − *Faculty of Chemistry, Jagiellonian University in Krakow, 30-387 Krakow, Poland*

Marek Rotko − *Department of Chemical Technology, Institute of Chemical Sciences, Faculty of Chemistry, Maria Curie-Sklodowska University, 20-031 Lublin, Poland*

Monika Ruszak − *Łukasiewicz Research Network - New Chemical Syntheses Institute, 24-110 Puławy, Poland*

Muhammad Fernadi Lukman − *Felix Bloch Institute for Solid State Physics, Universität Leipzig, 04103 Leipzig, Germany*

Ana Palčić − *Laboratory for the Synthesis of New Materials, Division of Materials Chemistry, Ruđer Bošković Institute, 10000 Zagreb, Croatia;* orcid.org/0000-0002-1092-4739

Reinhard Denecke − *Wilhelm-Ostwald-Institute of Physical and Theoretical Chemistry, Universität Leipzig, D-04103 Leipzig, Germany;* orcid.org/0000-0003-1065-5791

Marko Bertmer − *Felix Bloch Institute for Solid State Physics, Universität Leipzig, 04103 Leipzig, Germany;* orcid.org/0000-0002-3208-7927

Jacek Grams − *Institute of General and Ecological Chemistry, Faculty of Chemistry, Lodz University of Technology, 90-924 Lodz, Poland;* orcid.org/0000-0002-5087-7068

Andreas Pöppl − *Felix Bloch Institute for Solid State Physics, Universität Leipzig, 04103 Leipzig, Germany*

Roger Gläser − *Institute of Chemical Technology, Universität Leipzig, 04103 Leipzig, Germany;* orcid.org/0000-0002-8134-4280

Complete contact information is available at: https://pubs.acs.org/10.1021/acs.iecr.4c02245

Author Contributions

M.J.: Conceptualization, Methodology, Investigation, Data curation, Writing - original draft, Writing - review and editing, Supervision, Data management, Project management, Visualization, Resources. R.S.R.S.: Investigation, Data curation, Writing - review and editing, Data management. K.G.-M.: Investigation, Data curation, Writing - review and editing. M.R.: Data curation, Writing - review and editing. M.R.: Investigation, Review. M.F.L.: Investigation, Data curation, Writing - review and editing. A.P.: Writing - review and editing. R.D.: Investigation, Data curation, Review. M.B.: Investigation, Data curation. J.G.: Investigation, Data curation. A.P.: Review. R.G.: Review.

Notes

The authors declare no competing financial interest.

■ ACKNOWLEDGMENTS

M.J. acknowledges a DFG Research Grant JA 2998/2-1 and Zawacka NAWA programme for a Research Grant at the Łukasiewicz Research Network-New Chemical Syntheses Institute, Puławy, R.S.R.S. acknowledges the DAAD scholarship programme. A.P. acknowledges Croatian Science Foundation for funding, project ID: UIP-2019-04-4977. M.F.L. acknowledges a DFG Research Grant of GRK:2721 and thanks Dr. Winfried Böhlmann for the technical assistance on the dehydration procedure. K.G.-M. acknowledges the National Science Centre, Poland [Grant No. 2021/41/B/ST4/00048]. R.D. thanks Dr. Manuela Reichelt for help with the XPS experiments.

■ REFERENCES

(1) Jabłońska, M. Review of the Application of Cu-Containing SSZ-13 in NH_3-SCR-DeNO$_x$ and NH_3-SCO. *RSC Adv.* **2022**, *12* (39), 25240−25261.

(2) Jabłońska, M. Recent Progress in the Selective Catalytic Reduction of NO$_x$ with NH_3 on Cu-SAPO-34 Catalysts. *Molecular Catalysis* **2022**, *518*, No. 112111.

(3) Shi, Z.; Peng, Q.; E, J.; Xie, B.; Wei, J.; Yin, R.; Fu, G. Mechanism, Performance and Modification Methods for NH_3-SCR Catalysts: A Review. *Fuel* **2023**, *331*, No. 125885.

(4) Zhang, W.; Chen, J.; Guo, L.; Zheng, W.; Wang, G.; Zheng, S.; Wu, X. Research Progress on NH_3-SCR Mechanism of Metal-Supported Zeolite Catalysts. *J. Fuel Chem. Technol.* **2021**, *49*, 1294.

(5) Zhou, J.; Zhao, C.; Lin, J.; Yang, H.; Zhou, R. Promotional Effects of Cerium Modification of Cu-USY Catalysts on the Low-Temperature Activity of NH_3-SCR. *Catal. Commun.* **2018**, *114*, 60.

(6) Wan, J.; Yang, H.; Shi, Y.; Liu, Y.; Zhang, J.; Zhang, J.; Wu, G.; Zhou, R. Effect of Cu Loading Content on the Catalytic Performance of Cu-USY Catalysts for Selective Catalytic Reduction of NO with NH_3. *J. Environ. Sci.* **2023**, *126*, 445.

(7) Góra-Marek, K.; Tarach, K. A.; Piwowarska, Z.; Łaniecki, M.; Chmielarz, L. Ag-Loaded Zeolites Y and USY as Catalysts for Selective Ammonia Oxidation. *Catal. Sci. Technol.* **2016**, *6*, 1651.
(8) Suharbiansah, R. S. R.; Lukman, M. F.; Nannuzzi, C.; Wach, A.; Góra-Marek, K.; Liebau, M.; Palčić, A.; Pöppl, A.; Berlier, G.; Bordiga, S.; Gläser, R.; Jabłońska, M. Effect of the Preparation Method on the Catalytic Properties of Copper-Containing Zeolite Y Applied for NH_3-SCR-DeNO$_x$. *Catal. Sci. Technol.* **2023**, *13*, 3804.
(9) Suharbiansah, R. S. R.; Pyra, K.; Liebau, M.; Poppitz, D.; Góra-Marek, K.; Gläser, R.; Jabłońska, M. Micro-/Mesoporous Copper-Containing Zeolite Y Applied in NH_3-SCR, DeNO$_x$. *Microporous Mesoporous Mater.* **2022**, *334*, No. 111793.
(10) Verboekend, D.; Vilé, G.; Pérez-Ramírez, J. Hierarchical Y and USY Zeolites Designed by Post-Synthetic Strategies. *Adv. Funct. Mater.* **2012**, *22*, 916.
(11) Verboekend, D.; Pérez-Ramírez, J. Design of Hierarchical Zeolite Catalysts by Desilication. *Catal. Sci. Technol.* **2011**, *1*, 879.
(12) Zeolite Y. https://www.zeolyst.com/our-products/standard-zeolite-powders/zeolite-y.html (acessed July 2024).
(13) Verboekend, D.; Nuttens, N.; Locus, R.; Van Aelst, J.; Verolme, P.; Groen, J. C.; Pérez-Ramírez, J.; Sels, B. F. Synthesis, Characterisation, and Catalytic Evaluation of Hierarchical Faujasite Zeolites: Milestones, Challenges, and Future Directions. *Chem. Soc. Rev.* **2016**, *45*, 3331.
(14) Valtchev, V.; Majano, G.; Mintova, S.; Pérez-Ramírez, J. Tailored Crystalline Microporous Materials by Post-Synthesis Modification. *Chem. Soc. Rev.* **2013**, *42*, 263.
(15) Ray, G. J.; Meyers, B. L.; Marshall, C. L. ^{29}Si and ^{27}Al Nmr Study of Steamed Faujasites-Evidence for Non-Framework Tetrahedrally Bound Aluminium. *Zeolites* **1987**, *7*, 307.
(16) Xu, B.; Bordiga, S.; Prins, R.; van Bokhoven, J. A. Effect of Framework Si/Al Ratio and Extra-Framework Aluminum on the Catalytic Activity of Y Zeolite. *Appl. Catal. A: Gen.* **2007**, *333*, 245.
(17) Klinowski, J.; Thomas, J. M.; Audier, M.; Vasudevan, S.; Fyfe, C. A.; Hartman, J. S. Solid-State ^{29} Si Nmr and High-Resolution Electron Microscopic Studies of a Silicate Analogue of Faujasite. *J. Chem. Soc., Chem. Commun.* **1981**, *11*, 570.
(18) Kieger, S.; Delahay, G.; Coq, B.; Neveu, B. Selective Catalytic Reduction of Nitric Oxide by Ammonia over Cu-FAU Catalysts in Oxygen-Rich Atmosphere. *J. Catal.* **1999**, *183*, 267.
(19) Wang, H.; Xu, R.; Jin, Y.; Zhang, R. Zeolite Structure Effects on Cu Active Center, SCR Performance and Stability of Cu-Zeolite Catalysts. *Catal. Today* **2019**, *327*, 295.
(20) Tarach, K. A.; Jabłońska, M.; Pyra, K.; Liebau, M.; Reiprich, B.; Gläser, R.; Góra-Marek, K. Effect of Zeolite Topology on NH_3-SCR Activity and Stability of Cu-Exchanged Zeolites. *Appl. Catal. B: Environ.* **2021**, *284*, No. 119752.
(21) Bruzzese, P. C.; Salvadori, E.; Civalleri, B.; Jäger, S.; Hartmann, M.; Pöppl, A.; Chiesa, M. The Structure of Monomeric Hydroxo-Cu^{II} Species in Cu-CHA. A Quantitative Assessment. *J. Am. Chem. Soc.* **2022**, *144*, 13079.
(22) Jabłońska, M.; Suharbiansah, R. S. R.; Zhang, N.; Shimizu, K.; Lukman, M. F.; Bertmer, M.; Lei, H.; Pöppl, A.; Simon, U.; Gläser, R. Disclosing the Enhanced NH_3-SCR-DeNO$_x$ Activity of Cu-Containing Zeolite Y Prepared with 15-Crown-5. *Catal. Today* **2024**, *432*, No. 114611.
(23) Robles, A. M.; Deplano, G.; Góra-Marek, K.; Rotko, M.; Wach, A.; Lukman, M. F.; Bertmer, M.; Signorile, M.; Bordiga, S.; Pöppl, A.; Gläser, R.; Jabłońska, M. Post-Synthetically Treated ERI and SSZ-13 Zeolites Modified with Copper as Catalysts for NH_3-SCR-DeNO$_x$. *Catalysts* **2024**, *14*, 457.
(24) Aylor, A. W.; Larsen, S. C.; Reimer, J. A.; Bell, A. T. An Infrared Study of NO Decomposition over Cu-ZSM-5. *J. Catal.* **1995**, *157*, 592.
(25) Dedecek, J.; Sobalik, Z.; Tvaruazkova, Z.; Kaucky, D.; Wichterlova, B. Coordination of Cu Ions in High-Silica Zeolite Matrixes. Cu$^+$ Photoluminescence, IR of NO Adsorbed on Cu^{2+}, and Cu^{2+} ESR Study. *J. Phys. Chem.* **1995**, *99*, 16327.
(26) Fedyna, M.; Mozgawa, B.; Zasada, F.; Góra-Marek, K.; Gryboś, J.; Piskorz, W.; Yin, C.; Zhao, Z.; Pietrzyk, P.; Sojka, Z. Mechanistic Stages of the SCR Reaction-Insights into the Trade-off between NO Reduction and NH_3 Oxidation over CuSSZ-13 Catalysts via Isotopic $^{15}NH_3$ and $^{18}O_2$ TPSR and Steady State Studies Supported by IR 2D COS and DFT Modeling. *Appl. Catal. B: Environ.* **2023**, *325*, No. 122309.
(27) Mozgawa, B.; Zasada, F.; Fedyna, M.; Góra-Marek, K.; Tabor, E.; Mlekodaj, K.; Dědeček, J.; Zhao, Z.; Pietrzyk, P.; Sojka, Z. Analysis of NH_3-TPD Profiles for CuSSZ-13 SCR Catalyst of Controlled Al Distribution-Complexity Resolved by First Principles Thermodynamics of NH_3 Desorption, IR and EPR Insight into Cu Speciation. *Chem.—Eur. J.* **2021**, *27*, 17159.
(28) Hadjiivanov, K.; Saussey, J.; Freysz, J. L.; Lavalley, J. C. FT-IR Study of NO+O_2 Co-Adsorption on H-ZSM-5: Re-Assignment of the 2133 cm^{-1} Band to NO$^+$ Species. *Catal. Lett.* **1998**, *52*, 103.
(29) Hu, W.; Selleri, T.; Gramigni, F.; Fenes, E.; Rout, K. R.; Liu, S.; Nova, I.; Chen, D.; Gao, X.; Tronconi, E. On the Redox Mechanism of Low-Temperature NH_3-SCR over Cu-CHA: A Combined Experimental and Theoretical Study of the Reduction Half Cycle. *Angew. Chem., Int. Ed.* **2021**, *60*, 7197.
(30) Jabłońska, M. An Application of Steady-State Isotopic-Transient Kinetic Analysis (SSITKA) in DeNO$_x$ Process. *ChemCatChem.* **2021**, *13*, 818.
(31) Ledesma, C.; Yang, J.; Chen, D.; Holmen, A. Recent Approaches in Mechanistic and Kinetic Studies of Catalytic Reactions Using SSITKA Technique. *ACS Catal.* **2014**, *4*, 4527.

https://doi.org/10.1021/acs.iecr.4c02245
Ind. Eng. Chem. Res. 2024, 63, 17075−17085